CBFβ-SMMHC Affects Genome-wide Polycomb Repressive Complex 1 Activity in Acute Myeloid Leukemia

Gaëlle Cordonnier, Amit Mandoli, Nicolas Cagnard, Guillaume Hypolite, Ludovic Lhermitte, Els Verhoeyen, Vahid Asnafi, Niall Dillon, Elizabeth Macintyre, Joost H.A. Martens, et al.

Version of Record: https://www.sciencedirect.com/science/article/pii/S2211124719316766
Manuscript_b28c66ac7b9ebec0b5f7c885794e937d

CBFβ-SMMHC affects genome-wide Polycomb Repressive Complex 1 activity in Acute Myeloid Leukemia

Gaëlle Cordonnier[1,2], Amit Mandoli[3], Nicolas Cagnard[4], Guillaume Hypolite[1,2], Ludovic Lhermitte[1,2], Els Verhoeyen[5,6], Vahid Asnafi[1,2], Niall Dillon[7], Elizabeth Macintyre[1,2], Joost H.A. Martens[3], Jonathan Bond[1,2,8,9]

[1]Université Paris Descartes Sorbonne Cité, Institut Necker Enfants Malades (INEM), Institut national de recherche médicale (INSERM) U1151, [2]Laboratory of Onco-Hematology, Assistance Publique-Hôpitaux de Paris (AP-HP), Hôpital Necker-Enfants Malades, Paris, France, [3]Department of Molecular Biology, Faculty of Science, Nijmegen Centre for Molecular Life Sciences, Radboud University, Nijmegen, The Netherlands, [4]Sorbonne Universités, Université Paris Descartes, Bioinformatics Platform, Paris, France, [5]CIRI, International center for Infectiology Research, EVIR team, Université de Lyon, INSERM U1111, Lyon, France, [6]Université Côte d'Azur, INSERM, C3M, 06204 Nice, France, [7]Gene Regulation and Chromatin Group, MRC London Institute of Medical Sciences, Imperial College London, United Kingdom, [8]Systems Biology Ireland, School of Medicine, University College Dublin, [9]National Children's Research Centre, Children's Health Ireland at Crumlin, Dublin, Ireland.

Lead Contact and Correspondence: Jonathan Bond (jonathan.bond@ucd.ie)

Summary: Mutations and deletions of Polycomb Repressive Complex (PRC) components are increasingly recognized to affect tumor biology in a range of cancers. However, little is known about how genetic alterations of PRC-interacting molecules like the Core Binding Factor (CBF) complex influence Polycomb activity. We report that the acute myeloid leukemia (AML)-associated CBFβ-SMMHC fusion oncoprotein physically interacts with the PRC1 complex, and that these factors co-localize across the AML genome in an apparently PRC2-independent manner. Depletion of CBFβ-SMMHC caused substantial increases in genome-wide PRC1 binding and marked changes in the association between PRC1 and the CBF DNA-binding subunit RUNX1. PRC1 was more likely to be associated with actively transcribed genes in CBFβ-SMMHC-expressing cells. CBFβ-SMMHC depletion had heterogeneous effects on gene expression, including significant reductions in transcription of ribosomal loci occupied by PRC1. Our results provide evidence that CBFβ-SMMHC markedly and diversely affects Polycomb recruitment and transcriptional regulation across the AML genome.

Keywords: Acute Myeloid Leukemia, Core Binding Factor, Oncogene, Polycomb, Epigenetic Regulation.

Introduction:

Cancer-associated gene fusion products act as oncogenic drivers in a wide range of human malignancies (Gao et al., 2018; Mertens et al., 2015). These fusions have pleiotropic effects on tumor cell biology that frequently comprise subversion of the normal function of the involved wild-type (WT) factors (Mitelman et al., 2007). The acute myeloid leukemia (AML)-associated *CBFβ-MYH11* gene fusion is generated by chromosomal inversion inv(16)(p13.1q22) or translocation t(16;16)(p13.1q22) and gives rise to the CBFβ-SMMHC oncoprotein (Liu et al., 1993). WT CBFβ forms part of the heterodimeric Core Binding Factor (CBF) complex along with one of three tissue-specific DNA-binding RUNX proteins, which in hematopoietic cells is usually RUNX1 (Bravo et al., 2001). CBF is a critical regulator of multiple aspects of blood cell development (Kundu and Liu, 2003; Link et al., 2010; Speck and Gilliland, 2002), and the oncogenic effects of CBFβ-SMMHC are presumed to arise from subversion of WT CBF activities through several mechanisms. For example, CBFβ-SMMHC competes with WT CBFβ for RUNX1 binding and sequesters RUNX1 and RUNX-interacting proteins in the cytoplasm (Adya et al., 1998; Kanno et al., 1998; Wee et al., 2008). CBFβ-SMMHC is also present in the nucleus, and has been reported to alter RUNX1 target gene expression through recruitment of transcriptionally repressive histone deacetylases (HDACs) (Lutterbach et al., 1999). We have recently shown that CBFβ-SMMHC also frequently binds to actively transcribed genes along with RUNX1 and other chromatin factors, including the histone acetyltransferase EP300 (Mandoli et al., 2014), suggesting that CBFβ-SMMHC diversely affects epigenetic regulation of the leukemic transcriptome.

Perturbed epigenetic activity is increasingly recognized as a hallmark of human cancer, with roughly half of all malignancies having mutations or deletions in chromatin

modifiers (Shen and Laird, 2013; You and Jones, 2012). In particular, leukemias frequently harbor alterations in Polycomb factors (Iwama, 2017; Radulović et al., 2013) that mediate transcriptional regulation during normal hematopoiesis (Vidal and Starowicz, 2017). Polycomb group proteins predominantly act as epigenetic transcriptional repressors and function as part of multimeric complexes, of which the Polycomb Repressive Complexes PRC1 and PRC2 are the best described (Connelly and Dykhuizen, 2017; Margueron and Reinberg, 2011). In the canonical model of Polycomb activity, trimethylation of lysine 27 in the histone H3 tail (H3K27me3) by the PRC2 enzymatic subunit EZH1/2 causes recruitment of PRC1, leading to RING1-mediated ubiquitinylation of histone H2A (H2AK119ub), heterochromatin formation and inhibition of transcriptional elongation (Di Croce and Helin, 2013). As predicted by this model, PRC1 and PRC2 are usually found at the same genetic loci (Boyer et al., 2006; Bracken et al., 2006; Lee et al., 2006). However, an increasing number of non-canonical mechanisms of PRC1 recruitment are now recognized (Dietrich et al., 2012; Wu et al., 2013), and understanding of the diversity of mammalian Polycomb complex composition in different cellular contexts continues to evolve (Di Carlo et al., 2019).

Importantly in blood cells, the CBF complex has been shown to recruit PRC1 to chromatin through a PRC2-independent mechanism (Yu et al., 2012). It is therefore likely that PRC1 recruitment is affected in hematological cancers that harbor somatic mutations and translocations of either *RUNX1* and *CBFβ* which lead to subversion of WT CBF action (Sood et al., 2017). We decided to test this hypothesis in acute leukemia by evaluating the physical and functional interactions between Polycomb factors and the CBFβ-SMMHC oncoprotein in AML.

Results:

The CBFβ-SMMHC oncoprotein physically interacts with the PRC1 complex

We initially assessed the physical interaction between CBFβ-SMMHC and the PRC1 complex. Our previously reported SILAC (Stable Isotope Labeling by Amino acids in Culture) analysis had revealed a moderate interaction between the DNA-bound CBFβ-SMMHC/RUNX1 complex and the PRC1 component BMI-1 (Mandoli et al., 2014). To assess this further, we performed protein co-immunoprecipitation (Co-IP) experiments using extracts from the AML cell line ME-1, which expresses CBFβ-SMMHC. These cells also contain a tetracycline-inducible shRNA directed against *CBFβ-MYH11*, which we have previously used to assess oncoprotein-mediated gene regulation (Cordonnier et al., 2017; Mandoli et al., 2014).

IP with antibodies directed against RING1B (Figure 1A) and BMI-1 (Figure 1B) revealed that CBFβ-SMMHC interacts with each of these core components of the PRC1 complex. The specificity of the association was supported by the finding of marked reductions in the amounts of CBFβ-SMMHC detected in IP lysates following *CBFβ-MYH11* knockdown (KD) (Figures 1A and 1B). Increased amounts of WT CBFβ in IP lysates following shRNA KD were also evident. In contrast to previous reports in WT blood cells (Yu et al., 2012), we were unable to detect co-IP of RUNX1 with either RING1B or BMI-1. We additionally found that CBFβ-SMMHC co-IPed with both RING1B and BMI-1 in HeLa cells in which the oncoprotein was ectopically expressed (Figures 1C and 1D). Taken together, these data strongly suggest that CBFβ-SMMHC physically interacts with the PRC1 complex in AML cells.

CBFβ-SMMHC associates with the PRC1 complex across the AML genome

As CBFβ-SMMHC has been shown to sequester RUNX1 in the cytoplasm (Adya et al., 1998; Kanno et al., 1998), we considered whether PRC1 localization might also be modified in these cells, but immunofluorescence showed that both RING1B and BMI-1 were present in ME-1 cell nuclei (Supplemental Figure S2A).

We therefore reasoned that the physical association of the proteins most likely reflected interaction at the genomic level, so performed chromatin immunoprecipitation and massive parallel DNA sequencing (ChIP-seq) of CBFβ-SMMHC and RING1B in ME-1 cells. We complemented this analysis with ChIP-seq of RUNX1, which associates with CBFβ-SMMHC and shares the vast majority of genomic binding sites (Mandoli et al., 2014). These analyses revealed a major overlap in the localization of CBFβ-SMMHC, RING1B and RUNX1, whereby the vast majority of RING1B-bound sites (81%) were also occupied by the oncoprotein (Figure 2A).

We next performed gene ontology analysis of the peaks shared between CBFβ-SMMHC and RING1B. A selection of these commonly bound loci was confirmed in independent ChIP-QPCR experiments (Supplemental Figure S2B). Analysis using the GREAT tool (McLean et al., 2010) revealed that co-occupied loci frequently code for factors involved in RNA transcription and protein translation (Figure 2B). We have recently reported that CBFβ-SMMHC affects the regulation of these molecular pathways, and that ribosomal gene expression is significantly altered in CBFβ-SMMHC+ AML (Cordonnier et al., 2017). These new analyses showed that loci coding for ribosomal subunits and factors involved in translation were often co-occupied by CBFβ-SMMHC and RING1B (Figure 2C and Supplemental Figure S2C), indicating that PRC1 may participate in transcriptional regulation at these sites.

We have previously found that the ME-1 cell line provides a good model for assessment of CBFβ-SMMHC genomic localization, which correlates with that observed in primary AML samples (Mandoli et al., 2014). To test whether the detected overlap between CBFβ-SMMHC and RING1B localization also pertains *in vivo*, we performed patient-derived xenografts (PDX) in immunodeficient NSG-S mice (Wunderlich et al., 2010) and performed ChIP-seq of CBFβ-SMMHC and RING1B on Magnetic-activated cell sorting (MACS)-sorted blasts from leukemias derived from two separate patients (Supplemental Figure S2D). While the number of peaks detected in PDX samples was lower than in the corresponding ME-1 analysis (Supplemental Table S2), we found that 78.0% and 63.7% of CBFβ-SMMHC binding sites, and 74.0% and 69.2% of RING1B peaks detected in the two murine PDX samples were also found in ME-1 cells (Figure 2D). There was also a moderate variable overlap between CBFβ-SMMHC and RING1B binding in PDX samples, with 33.6% and 57.3% of RING1B peaks being co-occupied by CBFβ-SMMHC (Figure 2E). In addition, 87.8% of CBFβ-SMMHC sites and 56.1% of RING1B sites were shared between PDX samples (Figure 2F). Overall, these and previous data support the use of ME-1 cells as a satisfactory proxy for the evaluation of the genomic interaction between CBFβ-SMMHC and RING1B in human AML, and confirm co-localization of these factors at similar loci *in vivo*.

CBFβ-SMMHC affects genome-wide PRC1 localization

The physical association and large genomic overlap led us to examine whether CBFβ-SMMHC affects the genomic localization of PRC1. We evaluated this in an ME-1 cell line (Mandoli et al., 2014) in which inducible expression of a *CBFβ-MYH11*-directed shRNA caused marked reductions in CBFβ-SMMHC amounts (Supplemental Figure S3A) and genome-wide binding (Figure 3A).

ChIP-seq analysis revealed that genome-wide distribution of RING1B changed markedly following CBFβ-SMMHC depletion, with a 45% increase in detected peaks (Figure 3A) and significant rise in tag density (Figure 3B). We excluded that these findings reflected increased *RING1B* transcription or protein levels (Supplemental Figures S3B and S3C). Importantly, none of the 10,099 RING1B peaks detected exclusively after *CBFβ-MYH11* KD were present in either PDX sample (Supplemental Figure S3D). Taken together, these results suggest that PRC1 binding is strongly influenced by the presence of CBFβ-SMMHC, and provide support for the specificity of the ChIP-seq peaks detected in the xenografted leukemias.

We also found that CBFβ-SMMHC depletion caused major changes in the genomic association of RING1B and RUNX1. In the presence of the oncoprotein, 73.9% of RUNX1 peaks are co-occupied by RING1B (Figure 2A). This overlap increased further following *CBFβ-MYH11* KD, as RING1B was detected at nearly all (96.4%) RUNX1-bound regions (Figure 3C). Furthermore, a large proportion (56%) of RUNX1 sites not bound by RING1B in the presence of CBFβ-SMMHC were found to be co-occupied by RING1B following oncoprotein KD (Figure 3C, right), suggesting that the presence of CBFβ-SMMHC significantly modulates this interaction.

We then performed RNA-sequencing analysis of these experiments. In keeping with our previous data (Mandoli et al., 2014), there were varied changes in gene transcription following *CBFβ-MYH11* KD. Consistent with our previous report (Cordonnier et al., 2017), genes coding for ribosomal subunit proteins were frequently downregulated, and RING1B occupancy tended to be increased at these loci (Supplemental Figure S3E). However, as observed previously, large shifts in gene expression (>2-fold) in these experiments were more likely to comprise reductions (175) than increases (78) (Supplemental Table S3). Notably, we found that RING1B localized more frequently to actively transcribed genes. In the presence of CBFβ-SMMHC, RING1B-bound genes were significantly more likely to be expressed than loci where RING1B was absent (3650 expressed/4827 RING1B present, 75.6% v 5773 expressed/21691 RING1B absent, 26.6%, $p < 0.001$). When we combined these analyses with our ChIP-seq results, we also found that genes that were upregulated following CBFβ-SMMHC depletion had significant increases in RING1B occupancy, while levels of RUNX1 and the PRC2 component EZH2 did not change (Figure 3D, upper panel). Apart from the expected reductions in CBFβ-SMMHC occupancy following oncoprotein depletion, no significant alterations in binding of any tested factor were seen at downregulated loci (Figure 3D, lower panel). We additionally found that increases in gene expression strongly correlated with levels of H3K27 acetylation (H3K27Ac), suggesting that these transcriptional changes may be at least partly driven by redistribution of H3K27Ac that correlates with active promoter and enhancer elements (Figure 3D).

PRC1 localization in CBFβ-SMMHC-positive AML is mostly PRC2-independent

ChIP-seq analysis of the PRC2 component EZH2 showed that while nearly all EZH2 sites were shared with RING1B in ME-1 cells, the majority of RING1B peaks (60.6%) were not bound by EZH2 (Figure 4A). A similar pattern of overlap was seen in both PDX samples (Supplemental Figure S4). This suggests that most PRC1 recruitment in CBFβ-SMMHC+ AML may be PRC2-independent. We found that the overwhelming majority (95.7%) of these putative PRC2-independent sites were associated with RUNX1 and/or CBFβ-SMMHC (Figure 4B).

Further analysis of these experiments revealed no evidence of any significant functional interplay between CBFβ-SMMHC and EZH2. For example, *CBFβ-MYH11* KD resulted in minimal change in the genomic association of EZH2 with RING1B and RUNX1 (Figure 4C), and we did not detect physical interaction between CBFβ-SMMHC and EZH2 proteins, albeit in the context of incomplete EZH2 pulldown (Figure 4D). In addition, there were no differences in EZH2 occupancy of upregulated or downregulated genes (Figure 3D), while the transcription (Supplemental Figure S3B) and amounts of EZH2 protein (Supplemental Figure S3C) did not change after *CBFβ-MYH11* KD. Taken together, these results suggest that PRC2-mediated recruitment of PRC1 is not significantly affected by CBFβ-SMMHC.

Discussion:

While there is much current interest in how acquired mutations and deletions of Polycomb factors alter oncogenic molecular processes (Chan et al., 2018; Chan and Morey, 2019; Laugesen et al., 2016), WT PRC complexes must also affect cancer biology. Our results show that the CBFβ-SMMHC fusion oncoprotein significantly modulates PRC1 complex activity in AML, and suggest that subversion of WT Polycomb factor function may be a common hallmark of cancers that harbor genetic alterations of PRC-interacting molecules.

Polycomb proteins are now recognized as key biological actors in human cancers and in acute leukemias in particular (Iwama, 2017; Radulović et al., 2013). Polycomb factors can have either oncogenic and tumor suppressive activities in different malignancies, suggesting that PRC modulation of cancer biology is highly dependent on cellular context (Ernst et al., 2010; Morin et al., 2010; Ntziachristos et al., 2012; Sneeringer et al., 2010). To date, altered PRC1 activity in human cancers has most commonly been linked to increased expression of PRC1 complex subunits (Iwama, 2017). In keeping with this, PRC1 components have been shown to be oncogenic in experimental models (Jacobs et al., 1999a; Jacobs et al., 1999b), and to establish leukemic stem cell gene expression programs in myeloid progenitors (Yuan et al., 2011). In addition, non-canonical PRC1 complexes appear to be essential for AML stem cell activity (van den Boom et al., 2016). PRC1 has previously been shown to cooperate with oncogenic fusion proteins in leukemic transformation and progression (Boukarabila et al., 2009; Rizo et al., 2010), proving that Polycomb proteins can affect leukemogenesis even in the context of oncogene-driven transcriptional dysregulation.

In keeping with this, a recent report demonstrated that CBFβ-SMMHC locally inhibited RUNX1-mediated recruitment of PRC1 at *MYC* enhancers (Pulikkan et al., 2018). Pharmacological inhibition of the oncoprotein caused eviction of SWI-SNF complexes from the *MYC* locus and replacement with PRC1, leading to *MYC* repression and apoptosis. Our results add to these specific findings, as we show that CBFβ-SMMHC affects PRC1 localization at a genome-wide level in an apparently PRC2-independent manner. The fact that oncoprotein depletion caused major increases in global RING1B genomic occupancy and co-localization with RUNX1 suggests that CBFβ-SMMHC exerts widespread effects on PRC1 activity in human AML. In keeping with our previous results (Mandoli et al., 2014), the transcriptional effects of *CBFβ-MYH11* KD at individual loci were highly varied, but genes with the most marked changes were more frequently downregulated than upregulated. Interestingly, RING1B levels were significantly increased at loci that were upregulated after KD, and RING1B was globally more likely to be associated with active genes in this cellular context. It is likely that further exploration of binding of alternative Polycomb complexes such as PRC1.1 (van den Boom et al., 2016), which are more likely to associate with active genes, will shed further light on the mechanisms that underlie these transcriptional changes.

Among downregulated genes, we found that ribosomal subunit loci were frequently occupied by PRC1. We have previously reported that CBFβ-SMMHC alters ribosomal biogenesis (Cordonnier et al., 2017), and this was also one of the pathways that was most significantly deregulated following pharmaceutical inhibition of the oncoprotein (Pulikkan et al., 2018). Our latest results and other recent data suggest that these mechanisms are multifactorial, arising due to direct effects of PRC1 at ribosomal genes and altered activity of upstream regulators, most notably MYC.

CBFβ-SMMHC depletion led to increased co-localization of RUNX1 with PRC1, in keeping with the previously reported specific findings at the *MYC* locus, and of the general extensive RUNX1 redistribution that followed pharmaceutical oncoprotein inhibition (Pulikkan et al., 2018). The fact that a majority of RUNX1 sites not bound by RING1B in the presence of CBFβ-SMMHC were found to be co-occupied following oncoprotein depletion suggests that CBFβ-SMMHC partially inhibits the genomic interaction of RUNX1 and PRC1. As the transcriptional changes observed at these loci are varied, it is likely that gene expression is influenced by local chromatin architecture and the diverse effects of upstream molecules. More work is needed to determine how the presence of additional epigenetic regulators might alter expression at individual gene loci. It is well recognized that WT RUNX1 can interact functionally with a range of chromatin-modifying enzymes including HDACs (Guo and Friedman, 2011) and acetyltransferases (Kitabayashi et al., 1998). We have previously demonstrated that CBFβ-SMMHC is often found at loci with dynamic histone acetylation changes (Mandoli et al., 2014), suggesting that these effects might also modulate transcriptional phenotype in this setting.

While it is likely that subversion of RUNX1 function is a common underlying feature of CBF-altered AML, extrapolation of these specific results to other genetic backgrounds should be made with caution. Although we have previously found that haploinsufficiency of Polycomb components is common in AMLs that harbor CBF subunit translocations (Bond et al., 2018), co-occurrence of mutations in other epigenetic regulators such as the Polycomb interactors *ASXL1* and *ASXL2* vary greatly between RUNX1-RUNX1T1+ and CBFβ-SMMHC+ cases (Duployez et al., 2016), suggesting that specific mechanisms of epigenetic regulation differ between these common AML subsets. It is to be hoped that detailed mapping of Polycomb activity in

different genetic backgrounds will lead to a more precise understanding of cell context-specific epigenetic disruption in human leukemias and other cancers.

Acknowledgements: The Necker laboratory is supported by the Association Laurette Fugain, La ligue contre le Cancer and the INCa CARAMELE Translational Research and PhD programs. The Martens laboratory was supported by the European Union's Seventh Framework Programme (FP7/2007-2013) under grant agreement no. 282510-BLUEPRINT and the Dutch Cancer Foundation (KUN 2011-4937). JB was supported by a Kay Kendall Leukaemia Fund Intermediate Research Fellowship and by the National Children's Research Centre, Children's Health Ireland at Crumlin, Dublin, Ireland. ND was funded by the Medical Research Council UK. We thank Nicolas Goudin for assistance with immunofluorescence analysis. The Institut Necker Imaging Facility is supported by the Fondation ARC.

Author Contributions: Conceptualization, J.B., E.M. and J.M.**;** Investigation, G.C., A.M., G.H., J.B., and L.L.; Formal Analysis, NC.; Resources, E.V.; Writing - Original Draft, J.B. and J.M. Visualization, G.C. and J.B.; Supervision, E.M., N.D., J.B. and J.M.; Funding Acquisition, E.M., N.D., V.A., J.M. and J.B.

Declarations of Interest: The authors declare no conflict of interest.

Figure Legends:

Figure 1: The CBFβ-SMMHC oncoprotein physically interacts with the PRC1 complex. Protein lysates from ME-1 cells in the absence or presence of *CBFβ-MYH11* knockdown (KD) were subjected to immunoprecipitation (IP) with **(A)** anti-RING1B and **(B)** anti-BMI1 antibodies. The CBFβ-SMMHC fusion was detected with both anti-SMMHC and anti-CBFβ antibodies, while the latter antibody also detected wild-type CBFβ. Figures indicate relative quantification after shRNA KD. Panels **(C)** (anti-RING1B IP) and **(D)** (anti-BMI1 IP) show IPs in HeLa cells in which CBFβ-SMMHC was ectopically expressed. Short and long exposures are shown for the weaker anti-RING1B IP. The original Western Blot images for panels (A) and (B) are shown in Supplementary Figure S1.

Figure 2: CBFβ-SMMHC associates with the PRC1 complex across the AML genome. **(A)** Venn diagram (made using Biovenn (Hulsen et al., 2008)) showing overlap of CBFβ-SMMHC, RUNX1 and RING1B ChIP-seq peaks in ME-1 cells. **(B)** Ontology analysis of genomic binding sites shared by CBFβ-SMMHC and RING1B, analyzed using the GREAT tool (McLean et al., 2010). The top results for annotations of molecular function are listed. **(C)** ChIP-seq tracks showing CBFβ-SMMHC and RING1B presence at loci coding for ribosomal proteins. Images were generated using the University of California Santa Cruz Genome Browser tool (Kent et al., 2002). Arrows indicate transcriptional start sites and directions. **(D)** Comparison of CBFβ-SMMHC (left) and RING1B (right) binding sites in ChIP-seq analysis of murine patient-derived xenografts (PDX) and the ME-1 line. Percentages indicate the proportion of shared sites. **(E)** Venn diagram indicating percentage overlaps between CBFβ-SMMHC and RING1B peaks in PDX samples. **(F)** Comparison of CBFβ-SMMHC (left) and RING1B (right) sites in PDX samples.

Figure 3: CBFβ-SMMHC affects genome-wide PCR1 localization. (A) Relative changes in CBFβ-SMMHC, RUNX1 and RING1B peaks in the absence or presence of *CBFβ-MYH11* KD. **(B)** Heat maps showing tag densities in control and KD samples. **(C)** Comparison of overlap between RUNX1 and RING1B peaks in the absence or presence of KD (left upper and lower panels). The lower panel shows changes in binding of the subset of peaks that were bound by RUNX1, but not by RING1B, in control conditions. **(D)** Analysis of occupancy of the genes with the largest expression changes (>2-fold) following *CBFβ-MYH11* KD. Boxes comprise the 25th-75th percentiles and horizontal lines indicate the median. Whiskers extend to the 10th and 90th percentiles. Significant changes ($p < 0.001$ by Wilcoxon Rank Sum test) are indicated.

Figure 4: PRC1 localization in CBFβ-SMMHC+ AML is mostly PRC2-independent. (A) Venn diagrams depicting overlap in RING1B and EZH2 sites in ME-1 cells. **(B)** Analysis of CBFβ-SMMHC and RUNX1 binding at putative PRC2-independent RING1B sites, as defined by absence of EZH2. **(C)** Bar graphs depicting percentages of shared sites between EZH2 and each of CBFβ-SMMHC, RUNX1 and RING1B in the absence or presence of *CBFβ-MYH11* KD. Numbers indicate EZH2 peak counts in each case. **(D)** Anti-EZH2 IP of extracts from the ME-1 cell line.

STAR METHODS

LEAD CONTACT AND MATERIALS AVAILABILITY

Further information and requests for resources and reagents should be directed to and will be fulfilled by the Lead Contact, Jonathan Bond (jonathan.bond@ucd.ie). This study did not generate new unique reagents.

EXPERIMENTAL MODEL AND SUBJECT DETAILS

Cell lines: Modified ME-1 cell line containing a tetracycline-inducible shRNA directed against *CBFβ-MYH11* (Mandoli et al., 2014). The original ME-1 line was derived from a male patient with AML. HeLa cell line originally derived from a female patient with cervical cancer.

Animals: Murine patient-derived xenografts were performed in ten week-old female NSG-SGM3 (NOD.Cg-Prkdcscid Il2rgtm1Wjl Tg(CMV-IL3,CSF2,KITLG)1Eav/MloySzJ) mice, purchased from Charles Rivers laboratory (Bar Harbor, ME, USA). Mouse experiments were performed in accordance with European Union guidelines after approval of the protocols by the local ethical committee (Project number 2017020814103710).

METHOD DETAILS

Cell culture**:** The ME-1 inducible cell line was generated by transduction of ME-1 cells with an FH1tUTG lentiviral construct (kindly provided by Patrick W. B. Derksen, UMC Utrecht). Cells were grown in RPMI medium (Thermo Fisher Scientific) with 10% Fetal Bovine Serum (Hyclone, GE Healthcare). Expression of an shRNA that specifically targets the region spanning the fusion between *CBFβ* and *MYH11* sequences

(GAGACAGCTTCACGAGTATGACTCGAGTCATACTCGTGAAGCTGTCTC) was induced by addition of doxycycline hyclate (Sigma-aldrich) at 600ng/ml. HeLa cells were grown in DMEM medium with 10% FBS (both Thermo Fisher Scientific).

Protein Co-IP and immunoblotting: Cells were lysed using RIPA buffer containing protease inhibitor (Roche). For IP, antibodies were incubated with Dynabeads protein G (Invitrogen) for 40 minutes at room temperature. Following washing, protein extracts were incubated overnight at 4°C. Beads were washed in RIPA buffer and IP extracts were eluted by incubation in Laemmli buffer at 100°C for 5 minutes. Antibodies used for Co-IP and immunoblotting are listed in the Key Resources Table. Quantification of protein levels was performed using the Chemidoc XRS system and ImageLab software (Biorad), following normalization to ACTIN levels.

Cell transfection: For ectopic expression of CBFβ-MYH11, HeLa cells were transfected using Lipofectamine® 2000 (Thermo Fisher Scientific), according to the manufacturer's instructions. Transfections were performed using a pHEF1-TIG vector that contained a CBFβ-MYH11 cDNA amplified from the ME-1 cell line. Control cells were transfected with the corresponding empty GFP vector.

Immunofluorescent staining: Cells were attached to slides using poly-L-lysine 0.01% for 45 minutes at room temperature (RT), followed by fixation with formaldehyde 3.5% for 20 minutes and permeabilization with Triton X-100 1% for 5 minutes. Slides were incubated with anti-RING1B (1/100) and anti-SMMHC (1/50) antibodies (see Table S1A) overnight then probed with goat anti-mouse 555 Alexa red antibody (Life Technologies). Images were acquired on Carl Zeiss LSM 700 Confocal microscope with Zen 2011 software using 63x objectives at RT, and processed using ImageJ software (National Institutes of Health).

***Chromatin immunoprecipitation (ChIP)*:** Cells were crosslinked with 1% formaldehyde for 10 mins at room temperature. Crosslinking was quenched with 0.125 M glycine, then cells were washed with three buffers: (1) PBS with 1.5% BSA, (2) 0.25% Triton X 100, 1 mM EDTA pH 8, 50 mM HEPES pH 7.5, 140 mM NaCl, 10% Glycerol, 0.75% NP-40 (3) 200 mM NaCl, 1mM EDTA pH 8, 0.5 mM EGTA pH 8, 10 mM Tris-HCl. Pellets were re-suspended in ChIP incubation buffer (0.15% SDS, 1% Triton X-100, 150 mM NaCl, 1 mM EDTA pH 8, 0.5 mM EGTA pH 8, 10mM Tris-HCl) and sonicated using a Bioruptor® Pico sonicator (Diagenode) for 7 min at high power (30s ON, 30s OFF) in order to obtain an average length for DNA fragments of approximately 100-300 bp. The quality of the sonication was assessing using the 2100 Bioanalyzer machine (Agilent). Sonicated chromatin was centrifuged at maximum speed for 10 min and then incubated overnight at 4°C in incubation buffer (10 mM Tris pH 8, 150 mM NaCl, 1 mM EDTA, 0.5 mM EGTA, 0.15% SDS, 1% Triton X 100, 0.1% BSA), with Dynabeads Protein G and the antibody used for ChIP (see Key Resources Table for details, including citations of previous use for ChIP-sequencing). Beads were washed sequentially at 4˚C with a series of buffers: twice with a solution of composition 0.1% SDS, 0.1% sodium deoxycholate, 1% Triton X-100, 150 mM NaCl, 10mM Tris pH 8, TEE (10 mM Tris pH 8, 1mM EDTA and 0.5mM EGTA); once with a buffer of identical composition other than an increased concentration of NaCl (500 mM); once with a solution of composition 0.25 M LiCl, 0.5% DOC, 0.5% NP-40, TEE; and finally twice with TEE. All buffers to this point were supplemented with protease inhibitors. Precipitated chromatin was eluted with 200 ul of elution buffer (1% SDS, 0.1 M $NaHCO_3$, 10ul/ml RNAse A) at room temperature for 30 minutes. Samples were de-crosslinked at 65°C overnight in the presence of 200 mM NaCl, then treated with 0.2mg/ml of proteinase K (42°C for 2 hours). ChIP DNA was

purified using QiaQuick PCR Purification Kit (Qiagen, 28106). Primers used for ChIP-QPCR are shown in the Key Resources Table.

RNA preparation and QPCR: RNA was extracted using Trizol/ Chloroform and Qiagen RNeasy kits, with extraction protocols adapted according to cell numbers. For high-throughput sequencing, RNA concentration was measured with a Qubit fluorometer (Invitrogen). Ribosomal RNA was removed by Ribo-Zero rRNA Removal Kit (Epicentre) according to the manufacturer's instructions. 16 µl of purified RNA was fragmented by addition of 4 µl 5× fragmentation buffer (200 mM Tris-acetate pH 8.2, 500 mM potassium acetate and 150 mM magnesium acetate) and incubated at 94°C for exactly 90s. After ethanol precipitation, fragmented RNA was mixed with 5 µg random hexamers, followed by incubation at 70°C for 10 min and chilling on ice. We synthesized the first-strand cDNA with this RNA primer mix by adding 4 µl 5× first-strand buffer, 2 µl 100 mM DTT, 1 µl 10 mM dNTPs, 132 ng of actinomycin D, 200 U SuperScript III, followed by 2 h incubation at 48°C. First strand cDNA was purified by Qiagen mini elute column to remove dNTPs and eluted in 34 µl elution buffer. Second-strand cDNA was synthesized by adding 91.8 µl, 5 µg random hexamers, 4 µl of 5× first-strand buffer, 2 µl of 100 mM DTT, 4 µl of 10 mM dNTPs with dTTP replaced by dUTP, 30 µl of 5× second-strand buffer, 40 U of Escherichia coli DNA polymerase, 10 U of E. coli DNA ligase and 2 U of E. coli RNase H, and incubated at 16°C for 2 h followed by incubation with 10 U T4 polymerase at 16°C for 10 minutes. Double-stranded cDNA was purified by Qiagen mini elute column and used for library preparation as described in the KAPA HyperPrep protocol. We incubated 1 U USER (NEB) with adaptor-ligated cDNA at 37°C for 15 min followed by 5 min at 95°C before PCR. For RT-QPCR, 1µg of RNA was retrotranscribed using Superscript III (Life Technologies). QPCR was performed using either Taqman or

SYBR® Green PCR Master Mix (Both Life Technologies) using standard protocols. Primer and Probe sequences are detailed in the Key Resources Table.

***High-throughput sequencing and analysis*:** ChIP-seq and RNA-seq libraries were loaded on E-gel and a band corresponding to ~300 bp (DNA + Adaptor) was collected. After quality assessment, the eligible library was sequenced on the Illumina HiSeq 2000 machine and generated 42 to 52 bp tags. After read mapping to the hg19 reference genome using BWA (Li and Durbin, 2009) and removal of PCR duplicates by Picard *MarkDuplicates* option (http://broadinstitute.github.io/picard/), peak calling was conducted using MACS1.3.3(Zhang et al., 2008) at a *p*-value cutoff of 10^{-6}. Read counts for each putative region were enumerated and then normalized to RPKM (reads per kilobase of gene length per million reads) for visualization in heat maps or boxplots. For each base pair in the genome, the number of overlapping sequence reads was determined, averaged over a 10 bp window and visualized in the UCSC genome browser (http://genome.ucsc.edu). Gene ontology analysis was performed using the Genomic Regions Enrichment of Annotations Tool (GREAT (McLean et al., 2010)). Default statistical parameters were used to detect nearby genes (≤ 10kb). Ontology was defined by the GREAT program.

Murine patient-derived xenografts were performed in ten week-old female NSG-SGM3 (NOD.Cg-Prkdcscid Il2rgtm1Wjl Tg(CMV-IL3,CSF2,KITLG)1Eav/MloySzJ) mice, purchased from Charles Rivers laboratory (Bar Harbor, ME, USA). Mouse experiments were performed in accordance with European Union guidelines after approval of the protocols by the local ethical committee (Project number 2017020814103710). Primary AML cells were obtained from two patients, referred to here as PDX1 and PDX2. Clinical details are shown in Supplemental Table S4. Mice were injected intra-tibially with 1.5 - 3

x 10^6 primary AML cells 24 hours after sublethal irradiation (0.5cGy for 30 seconds). Mice were sacrificed when chimerism levels in the bone marrow exceeded 70%, or if deemed humanely necessary.

QUANTIFICATION AND STATISTICAL ANALYSIS

Statistical analyses: Figure 3D: Wilcoxon signed-rank test to test differences in factor occupancy of loci with largest expression changes (>2-fold) following *CBFβ-MYH11* KD. n= 2 RNA-seq replicates and n = 1 for each ChIP-sequencing replicate (WT and post-knockdown). Boxes comprise the 25th-75th percentiles and horizontal lines indicate the median. Whiskers extend to the 10th and 90th percentiles.

Results section: Fisher's exact test was used to test differences in individual gene expression between RNA-seq replicates (n = 2) and RING1B occupancy of expressed and non-expressed loci (n = 1 for each ChIP-sequencing replicate).

Software: BWA (Li and Durbin, 2009), Picard *MarkDuplicates* (http://broadinstitute.github.io/picard/), MACS1.3.3 (Zhang et al., 2008) Genomic Regions Enrichment of Annotations Tool (GREAT (McLean et al., 2010)), as detailed in the methods section (high-throughput sequencing and analysis) and Key Resources Table.

DATA AND CODE AVAILABILITY

ChIP-seq and RNA-seq data files have been uploaded to the Gene Expression Omnibus with the associated GSE GSE128771.

KEY RESOURCES TABLE

REAGENT or RESOURCE	SOURCE	IDENTIFIER
Antibodies		
SMMHC (Mandoli et al., 2014)	Novus Biologicals	Cat#21370002
RUNX1 (Martens et al., 2012; Tijssen et al., 2011; Wilson et al., 2010; Yu et al., 2012)	Abcam	Cat#ab23980
CBFβ	Abcam	Cat#ab33516
RING1B (Landeira et al., 2010; Mendenhall et al., 2010)	MBL Life Science	Cat#D139-3
BMI1	Active Motif	Cat#39994
EZH2 (Chng et al., 2012; Inoue et al., 2013; Knutson et al., 2014; Kumar and Duester, 2014; Tong et al., 2014)	Active Motif	Cat#39901
ACTIN	Abcam	Cat#ab3280
Normal mouse IgG	Santa Cruz	Cat#sc-2025
Normal rabbit IgG	Santa Cruz	Cat#sc-2027
Biological Samples		
Patient-derived xenografts (PDX)	Local samples	See methods.
Critical Commercial Assays		
EZH2 Taqman QPCR assay	ThermoFisher	Hs01016789_m1
EED Taqman QPCR assay	ThermoFisher	Hs00537777_m1
SUZ12 Taqman QPCR assay	ThermoFisher	Hs00248742_m1
Deposited Data		
ChIP-seq and RNA-seq data	This paper	GEO: GSE128771
Experimental Models: Cell Lines		
ME-1 line with inducible shRNA against CBFβ-MYH11	(Mandoli et al., 2014)	N/A
HeLa cell line	DSMZ	Cat#ACC57
Experimental Models: Organisms/Strains		
Mouse: NSG-SGM3 (NOD.Cg-Prkdc^{scid} Il2rgtm1Wjl Tg(CMV-IL3,CSF2,KITLG)1Eav/MloySzJ)	Charles River Laboratories	JAX™ strain code: 013062
Oligonucleotides		
See Table S1 for full details.		

Recombinant DNA		
pHEF1-TIG-CBFβ-MYH11	Cloned locally	N/A
Software and Algorithms		
BWA	(Li and Durbin, 2009)	http://bio-bwa.sourceforge.net/
Picard MarkDuplicates option	N/A	http://broadinstitute.github.io/picard/
MACS1.3.3	(Zhang et al., 2008)	http://liulab.dfci.harvard.edu/MACS/
Genomic Regions Enrichment of Annotations Tool (GREAT)	(McLean et al., 2010)).	http://great.stanford.edu/public/html/

References:

Adya, N., Stacy, T., Speck, N.A., and Liu, P.P. (1998). The Leukemic Protein Core Binding Factor β (CBFβ)–Smooth-Muscle Myosin Heavy Chain Sequesters CBFα2 into Cytoskeletal Filaments and Aggregates. Molecular and Cellular Biology *18*, 7432-7443.

Bond, J., Labis, E., Marceau-Renaut, A., Duployez, N., Labopin, M., Hypolite, G., Michel, G., Ducassou, S., Boutroux, H., Nelken, B.*, et al.* (2018). Polycomb repressive complex 2 haploinsufficiency identifies a high-risk subgroup of pediatric acute myeloid leukemia. Leukemia *32*, 1878-1882.

Boukarabila, H., Saurin, A.J., Batsché, E., Mossadegh, N., van Lohuizen, M., Otte, A.P., Pradel, J., Muchardt, C., Sieweke, M., and Duprez, E. (2009). The PRC1 Polycomb group complex interacts with PLZF/RARA to mediate leukemic transformation. Genes & Development *23*, 1195-1206.

Boyer, L.A., Plath, K., Zeitlinger, J., Brambrink, T., Medeiros, L.A., Lee, T.I., Levine, S.S., Wernig, M., Tajonar, A., Ray, M.K.*, et al.* (2006). Polycomb complexes repress developmental regulators in murine embryonic stem cells. Nature *441*, 349-353.

Bracken, A.P., Dietrich, N., Pasini, D., Hansen, K.H., and Helin, K. (2006). Genome-wide mapping of Polycomb target genes unravels their roles in cell fate transitions. Genes & Development *20*, 1123-1136.

Bravo, J., Li, Z., Speck, N.A., and Warren, A.J. (2001). The leukemia-associated AML1 (Runx1)--CBF beta complex functions as a DNA-induced molecular clamp. Nature Structural Biology *8*, 371-378.

Chan, H.L., Beckedorff, F., Zhang, Y., Garcia-Huidobro, J., Jiang, H., Colaprico, A., Bilbao, D., Figueroa, M.E., LaCava, J., Shiekhattar, R.*, et al.* (2018). Polycomb complexes associate with enhancers and promote oncogenic transcriptional programs in cancer through multiple mechanisms. Nat Commun *9*, 3377.

Chan, H.L., and Morey, L. (2019). Emerging Roles for Polycomb-Group Proteins in Stem Cells and Cancer. Trends Biochem Sci.

Chng, K.R., Chang, C.W., Tan, S.K., Yang, C., Hong, S.Z., Sng, N.Y.W., and Cheung, E. (2012). A transcriptional repressor co-regulatory network governing androgen response in prostate cancers. The EMBO journal *31*, 2810-2823.

Connelly, K.E., and Dykhuizen, E.C. (2017). Compositional and functional diversity of canonical PRC1 complexes in mammals. Biochimica Et Biophysica Acta *1860*, 233-245.

Cordonnier, G., Mandoli, A., Radhouane, A., Hypolite, G., Lhermitte, L., Belhocine, M., Asnafi, V., Macintyre, E., Martens, J.H.A., Fumagalli, S.*, et al.* (2017). CBFbeta-SMMHC regulates ribosomal gene transcription and alters ribosome biogenesis. Leukemia *31*, 1443-1446.

Di Carlo, V., Mocavini, I., and Di Croce, L. (2019). Polycomb complexes in normal and malignant hematopoiesis. J Cell Biol *218*, 55-69.

Di Croce, L., and Helin, K. (2013). Transcriptional regulation by Polycomb group proteins. Nat Struct Mol Biol *20*, 1147-1155.

Dietrich, N., Lerdrup, M., Landt, E., Agrawal-Singh, S., Bak, M., Tommerup, N., Rappsilber, J., Södersten, E., and Hansen, K. (2012). REST-mediated recruitment of polycomb repressor complexes in mammalian cells. PLoS genetics *8*, e1002494.

Duployez, N., Marceau-Renaut, A., Boissel, N., Petit, A., Bucci, M., Geffroy, S., Lapillonne, H., Renneville, A., Ragu, C., Figeac, M.*, et al.* (2016). Comprehensive mutational profiling of core binding factor acute myeloid leukemia. Blood *127*, 2451-2459.

Ernst, T., Chase, A.J., Score, J., Hidalgo-Curtis, C.E., Bryant, C., Jones, A.V., Waghorn, K., Zoi, K., Ross, F.M., Reiter, A.*, et al.* (2010). Inactivating mutations of the histone methyltransferase gene EZH2 in myeloid disorders. Nature genetics *42*, 722-726.

Gao, Q., Liang, W.W., Foltz, S.M., Mutharasu, G., Jayasinghe, R.G., Cao, S., Liao, W.W., Reynolds, S.M., Wyczalkowski, M.A., Yao, L.*, et al.* (2018). Driver Fusions and Their Implications in the Development and Treatment of Human Cancers. Cell Rep *23*, 227-238 e223.

Guo, H., and Friedman, A.D. (2011). Phosphorylation of RUNX1 by cyclin-dependent kinase reduces direct interaction with HDAC1 and HDAC3. J Biol Chem *286*, 208-215.

Hulsen, T., de Vlieg, J., and Alkema, W. (2008). BioVenn â€“ a web application for the comparison and visualization of biological lists using area-proportional Venn diagrams, pp. 488.

Inoue, D., Kitaura, J., Togami, K., Nishimura, K., Enomoto, Y., Uchida, T., Kagiyama, Y., Kawabata, K.C., Nakahara, F., Izawa, K.*, et al.* (2013). Myelodysplastic syndromes are

induced by histone methylation–altering ASXL1 mutations. The Journal of Clinical Investigation *123*, 4627-4640.

Iwama, A. (2017). Polycomb repressive complexes in hematological malignancies. Blood *130*, 23-29.

Jacobs, J.J., Kieboom, K., Marino, S., DePinho, R.A., and van Lohuizen, M. (1999a). The oncogene and Polycomb-group gene bmi-1 regulates cell proliferation and senescence through the ink4a locus. Nature *397*, 164-168.

Jacobs, J.J., Scheijen, B., Voncken, J.W., Kieboom, K., Berns, A., and van Lohuizen, M. (1999b). Bmi-1 collaborates with c-Myc in tumorigenesis by inhibiting c-Myc-induced apoptosis via INK4a/ARF. Genes & Development *13*, 2678-2690.

Kanno, Y., Kanno, T., Sakakura, C., Bae, S.C., and Ito, Y. (1998). Cytoplasmic sequestration of the polyomavirus enhancer binding protein 2 (PEBP2)/core binding factor alpha (CBFalpha) subunit by the leukemia-related PEBP2/CBFbeta-SMMHC fusion protein inhibits PEBP2/CBF-mediated transactivation. Molecular and Cellular Biology *18*, 4252-4261.

Kent, W.J., Sugnet, C.W., Furey, T.S., Roskin, K.M., Pringle, T.H., Zahler, A.M., and Haussler, D. (2002). The human genome browser at UCSC. Genome research *12*, 996-1006.

Kitabayashi, I., Yokoyama, A., Shimizu, K., and Ohki, M. (1998). Interaction and functional cooperation of the leukemia-associated factors AML1 and p300 in myeloid cell differentiation. EMBO J *17*, 2994-3004.

Knutson, S.K., Kawano, S., Minoshima, Y., Warholic, N.M., Huang, K.-C., Xiao, Y., Kadowaki, T., Uesugi, M., Kuznetsov, G., Kumar, N.*, et al.* (2014). Selective inhibition of EZH2 by EPZ-6438 leads to potent antitumor activity in EZH2-mutant non-Hodgkin lymphoma. Molecular Cancer Therapeutics *13*, 842-854.

Kumar, S., and Duester, G. (2014). Retinoic acid controls body axis extension by directly repressing Fgf8 transcription. Development (Cambridge, England) *141*, 2972-2977.

Kundu, M., and Liu, P.P. (2003). Cbf beta is involved in maturation of all lineages of hematopoietic cells during embryogenesis except erythroid. Blood Cells, Molecules & Diseases *30*, 164-169.

Landeira, D., Sauer, S., Poot, R., Dvorkina, M., Mazzarella, L., Jørgensen, H.F., Pereira, C.F., Leleu, M., Piccolo, F.M., Spivakov, M.*, et al.* (2010). Jarid2 is a PRC2 component in embryonic stem cells required for multi-lineage differentiation and recruitment of PRC1 and RNA Polymerase II to developmental regulators. Nature Cell Biology *12*, 618-624.

Laugesen, A., Hojfeldt, J.W., and Helin, K. (2016). Role of the Polycomb Repressive Complex 2 (PRC2) in Transcriptional Regulation and Cancer. Cold Spring Harb Perspect Med *6*.

Lee, T.I., Jenner, R.G., Boyer, L.A., Guenther, M.G., Levine, S.S., Kumar, R.M., Chevalier, B., Johnstone, S.E., Cole, M.F., Isono, K.-i.*, et al.* (2006). Control of developmental regulators by Polycomb in human embryonic stem cells. Cell *125*, 301-313.

Li, H., and Durbin, R. (2009). Fast and accurate short read alignment with Burrows-Wheeler transform. Bioinformatics *25*, 1754-1760.

Link, K.A., Chou, F.-S., and Mulloy, J.C. (2010). Core binding factor at the crossroads: determining the fate of the HSC. Journal of Cellular Physiology *222*, 50-56.

Liu, P., Tarle, S., Hajra, A., Claxton, D., Marlton, P., Freedman, M., Siciliano, M., and Collins, F. (1993). Fusion between transcription factor CBF beta/PEBP2 beta and a myosin heavy chain in acute myeloid leukemia. Science *261*, 1041-1044.

Lutterbach, B., Hou, Y., Durst, K.L., and Hiebert, S.W. (1999). The inv(16) encodes an acute myeloid leukemia 1 transcriptional corepressor. Proceedings of the National Academy of Sciences of the United States of America *96*, 12822-12827.

Mandoli, A., Singh, A.A., Jansen, P.W.T.C., Wierenga, A.T.J., Riahi, H., Franci, G., Prange, K., Saeed, S., Vellenga, E., Vermeulen, M.*, et al.* (2014). CBFB-MYH11/RUNX1 together with a compendium of hematopoietic regulators, chromatin modifiers and basal transcription factors occupies self-renewal genes in inv(16) acute myeloid leukemia. Leukemia *28*, 770-778.

Margueron, R., and Reinberg, D. (2011). The Polycomb complex PRC2 and its mark in life. Nature *469*, 343-349.

Martens, J.H.A., Mandoli, A., Simmer, F., Wierenga, B.-J., Saeed, S., Singh, A.A., Altucci, L., Vellenga, E., and Stunnenberg, H.G. (2012). ERG and FLI1 binding sites demarcate targets for aberrant epigenetic regulation by AML1-ETO in acute myeloid leukemia. Blood *120*, 4038-4048.

McLean, C.Y., Bristor, D., Hiller, M., Clarke, S.L., Schaar, B.T., Lowe, C.B., Wenger, A.M., and Bejerano, G. (2010). GREAT improves functional interpretation of cis-regulatory regions. Nature Biotechnology *28*, 495-501.

Mendenhall, E.M., Koche, R.P., Truong, T., Zhou, V.W., Issac, B., Chi, A.S., Ku, M., and Bernstein, B.E. (2010). GC-rich sequence elements recruit PRC2 in mammalian ES cells. PLoS genetics *6*, e1001244.

Mertens, F., Johansson, B., Fioretos, T., and Mitelman, F. (2015). The emerging complexity of gene fusions in cancer. Nat Rev Cancer *15*, 371-381.

Mitelman, F., Johansson, B., and Mertens, F. (2007). The impact of translocations and gene fusions on cancer causation. Nat Rev Cancer *7*, 233-245.

Morin, R.D., Johnson, N.A., Severson, T.M., Mungall, A.J., An, J., Goya, R., Paul, J.E., Boyle, M., Woolcock, B.W., Kuchenbauer, F.*, et al.* (2010). Somatic mutations altering EZH2 (Tyr641) in follicular and diffuse large B-cell lymphomas of germinal-center origin. Nature genetics *42*, 181-185.

Ntziachristos, P., Tsirigos, A., Van Vlierberghe, P., Nedjic, J., Trimarchi, T., Flaherty, M.S., Ferres-Marco, D., da Ros, V., Tang, Z., Siegle, J.*, et al.* (2012). Genetic inactivation of the polycomb repressive complex 2 in T cell acute lymphoblastic leukemia. Nature medicine *18*, 298-301.

Pulikkan, J.A., Hegde, M., Ahmad, H.M., Belaghzal, H., Illendula, A., Yu, J., O'Hagan, K., Ou, J., Muller-Tidow, C., Wolfe, S.A.*, et al.* (2018). CBFbeta-SMMHC Inhibition Triggers Apoptosis by Disrupting MYC Chromatin Dynamics in Acute Myeloid Leukemia. Cell *174*, 172-186 e121.

Radulović, V., de Haan, G., and Klauke, K. (2013). Polycomb-group proteins in hematopoietic stem cell regulation and hematopoietic neoplasms. Leukemia *27*, 523-533.

Rizo, A., Horton, S.J., Olthof, S., Dontje, B., Ausema, A., van Os, R., van den Boom, V., Vellenga, E., de Haan, G., and Schuringa, J.J. (2010). BMI1 collaborates with BCR-ABL in leukemic transformation of human CD34+ cells. Blood *116*, 4621-4630.

Shen, H., and Laird, P.W. (2013). Interplay between the cancer genome and epigenome. Cell *153*, 38-55.

Sneeringer, C.J., Scott, M.P., Kuntz, K.W., Knutson, S.K., Pollock, R.M., Richon, V.M., and Copeland, R.A. (2010). Coordinated activities of wild-type plus mutant EZH2 drive tumor-associated hypertrimethylation of lysine 27 on histone H3 (H3K27) in human B-cell lymphomas. Proc Natl Acad Sci U S A *107*, 20980-20985.

Sood, R., Kamikubo, Y., and Liu, P. (2017). Role of RUNX1 in hematological malignancies. Blood *129*, 2070-2082.

Speck, N.A., and Gilliland, D.G. (2002). Core-binding factors in haematopoiesis and leukaemia. Nature Reviews Cancer *2*, 502-513.

Tijssen, M.R., Cvejic, A., Joshi, A., Hannah, R.L., Ferreira, R., Forrai, A., Bellissimo, D.C., Oram, S.H., Smethurst, P.A., Wilson, N.K.*, et al.* (2011). Genome-wide analysis of simultaneous GATA1/2, RUNX1, FLI1, and SCL binding in megakaryocytes identifies hematopoietic regulators. Developmental Cell *20*, 597-609.

Tong, Q., He, S., Xie, F., Mochizuki, K., Liu, Y., Mochizuki, I., Meng, L., Sun, H., Zhang, Y., Guo, Y.*, et al.* (2014). Ezh2 regulates transcriptional and posttranslational expression of T-bet and promotes Th1 cell responses mediating aplastic anemia in mice. Journal of Immunology (Baltimore, Md: 1950) *192*, 5012-5022.

van den Boom, V., Maat, H., Geugien, M., Rodriguez Lopez, A., Sotoca, A.M., Jaques, J., Brouwers-Vos, A.Z., Fusetti, F., Groen, R.W., Yuan, H.*, et al.* (2016). Non-canonical PRC1.1 Targets Active Genes Independent of H3K27me3 and Is Essential for Leukemogenesis. Cell Rep *14*, 332-346.

Vidal, M., and Starowicz, K. (2017). Polycomb complexes PRC1 and their function in hematopoiesis. Exp Hematol *48*, 12-31.

Wee, H.-J., Voon, D.C.-C., Bae, S.-C., and Ito, Y. (2008). PEBP2-beta/CBF-beta-dependent phosphorylation of RUNX1 and p300 by HIPK2: implications for leukemogenesis. Blood *112*, 3777-3787.

Wilson, N.K., Foster, S.D., Wang, X., Knezevic, K., Schütte, J., Kaimakis, P., Chilarska, P.M., Kinston, S., Ouwehand, W.H., Dzierzak, E.*, et al.* (2010). Combinatorial transcriptional control in blood stem/progenitor cells: genome-wide analysis of ten major transcriptional regulators. Cell Stem Cell *7*, 532-544.

Wu, X., Johansen, J.V., and Helin, K. (2013). Fbxl10/Kdm2b recruits polycomb repressive complex 1 to CpG islands and regulates H2A ubiquitylation. Molecular Cell *49*, 1134-1146.

Wunderlich, M., Chou, F.-S., Link, K.A., Mizukawa, B., Perry, R.L., Carroll, M., and Mulloy, J.C. (2010). AML xenograft efficiency is significantly improved in NOD/SCID-IL2RG mice constitutively expressing human SCF, GM-CSF and IL-3. Leukemia *24*, 1785-1788.

You, J.S., and Jones, P.A. (2012). Cancer genetics and epigenetics: two sides of the same coin? Cancer Cell *22*, 9-20.

Yu, M., Mazor, T., Huang, H., Huang, H.-T., Kathrein, K.L., Woo, A.J., Chouinard, C.R., Labadorf, A., Akie, T.E., Moran, T.B.*, et al.* (2012). Direct recruitment of polycomb repressive complex 1 to chromatin by core binding transcription factors. Molecular Cell *45*, 330-343.

Yuan, J., Takeuchi, M., Negishi, M., Oguro, H., Ichikawa, H., and Iwama, A. (2011). Bmi1 is essential for leukemic reprogramming of myeloid progenitor cells. Leukemia *25*, 1335-1343.

Zhang, Y., Liu, T., Meyer, C.A., Eeckhoute, J., Johnson, D.S., Bernstein, B.E., Nusbaum, C., Myers, R.M., Brown, M., Li, W.*, et al.* (2008). Model-based analysis of ChIP-Seq (MACS). Genome Biol *9*, R137.

Figure 1

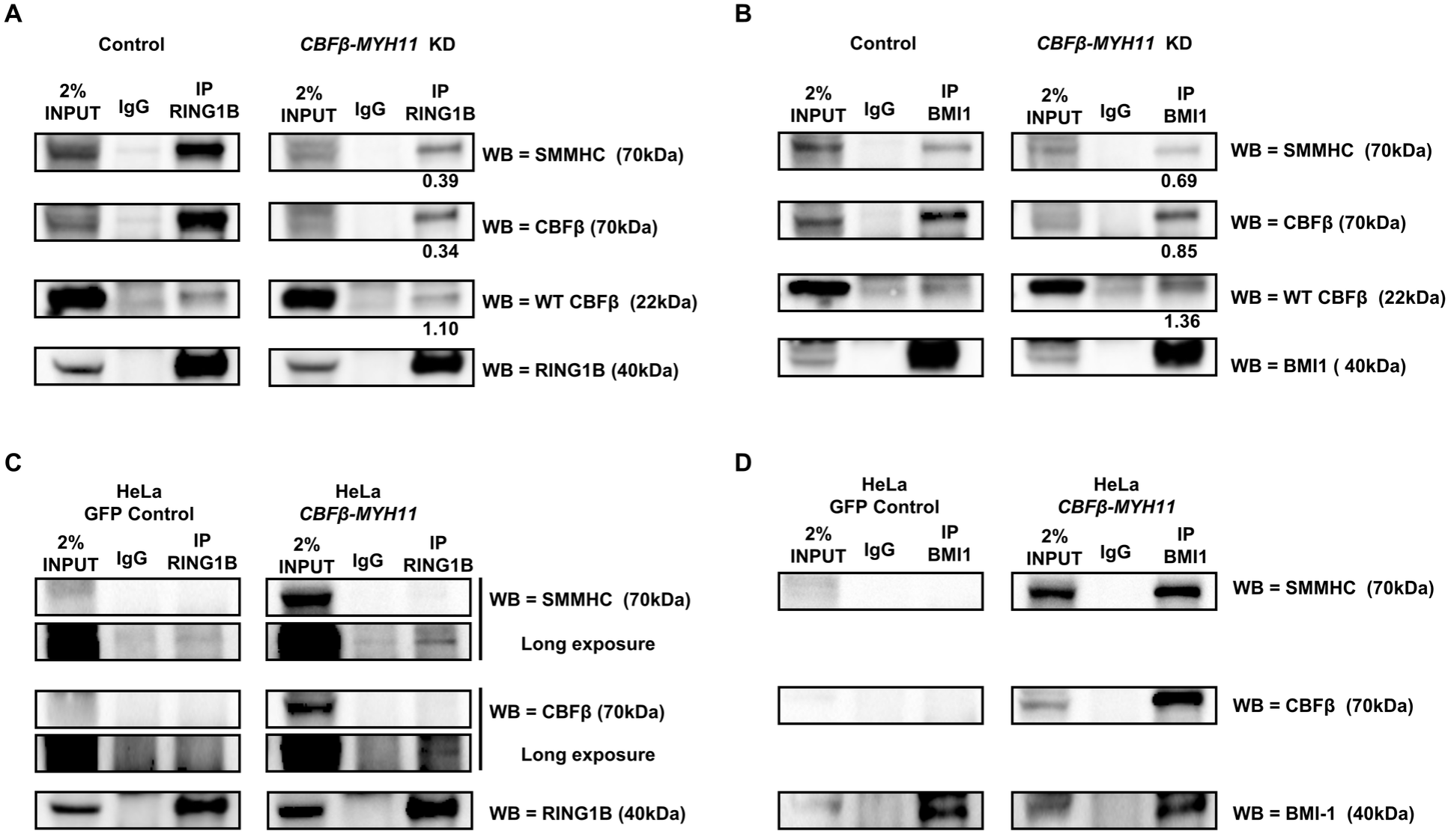
A
Control
CBFβ-MYH11 KD
2% INPUT
IgG
IP RING1B
WB = SMMHC (70kDa)
0.39
WB = CBFβ (70kDa)
0.34
WB = WT CBFβ (22kDa)
1.10
WB = RING1B (40kDa)
B
Control
CBFβ-MYH11 KD
2% INPUT
IgG
IP BMI1
WB = SMMHC (70kDa)
0.69
WB = CBFβ (70kDa)
0.85
WB = WT CBFβ (22kDa)
1.36
WB = BMI1 (40kDa)
C
HeLa GFP Control
HeLa CBFβ-MYH11
2% INPUT
IgG
IP RING1B
WB = SMMHC (70kDa)
Long exposure
WB = CBFβ (70kDa)
Long exposure
WB = RING1B (40kDa)
D
HeLa GFP Control
HeLa CBFβ-MYH11
2% INPUT
IgG
IP BMI1
WB = SMMHC (70kDa)
WB = CBFβ (70kDa)
WB = BMI-1 (40kDa)

Figure 2

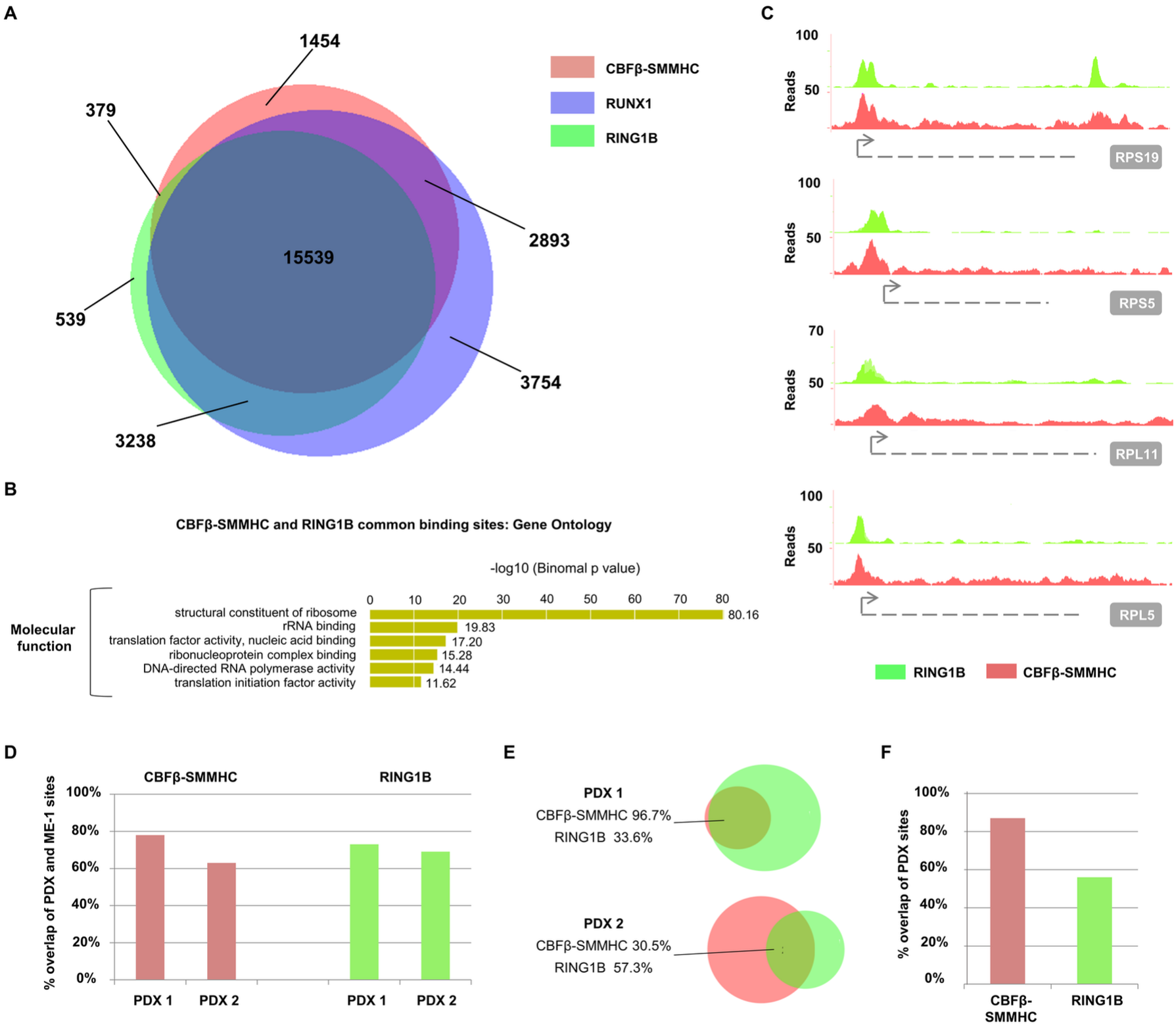
A
1454
379
2893
15539
539
3754
3238
CBFβ-SMMHC
RUNX1
RING1B
B
CBFβ-SMMHC and RING1B common binding sites: Gene Ontology
-log10 (Binomal p value)
0 10 20 30 40 50 60 70 80
Molecular function
structural constituent of ribosome 80.16
rRNA binding 19.83
translation factor activity, nucleic acid binding 17.20
ribonucleoprotein complex binding 15.28
DNA-directed RNA polymerase activity 14.44
translation initiation factor activity 11.62
C
Reads
RPS19
RPS5
RPL11
RPL5
RING1B
CBFβ-SMMHC
D
CBFβ-SMMHC
RING1B
% overlap of PDX and ME-1 sites
100%
80%
60%
40%
20%
0%
PDX 1
PDX 2
PDX 1
PDX 2
E
PDX 1
CBFβ-SMMHC 96.7%
RING1B 33.6%
PDX 2
CBFβ-SMMHC 30.5%
RING1B 57.3%
F
% overlap of PDX sites
100%
80%
60%
40%
20%
0%
CBFβ-SMMHC
RING1B

Figure 3

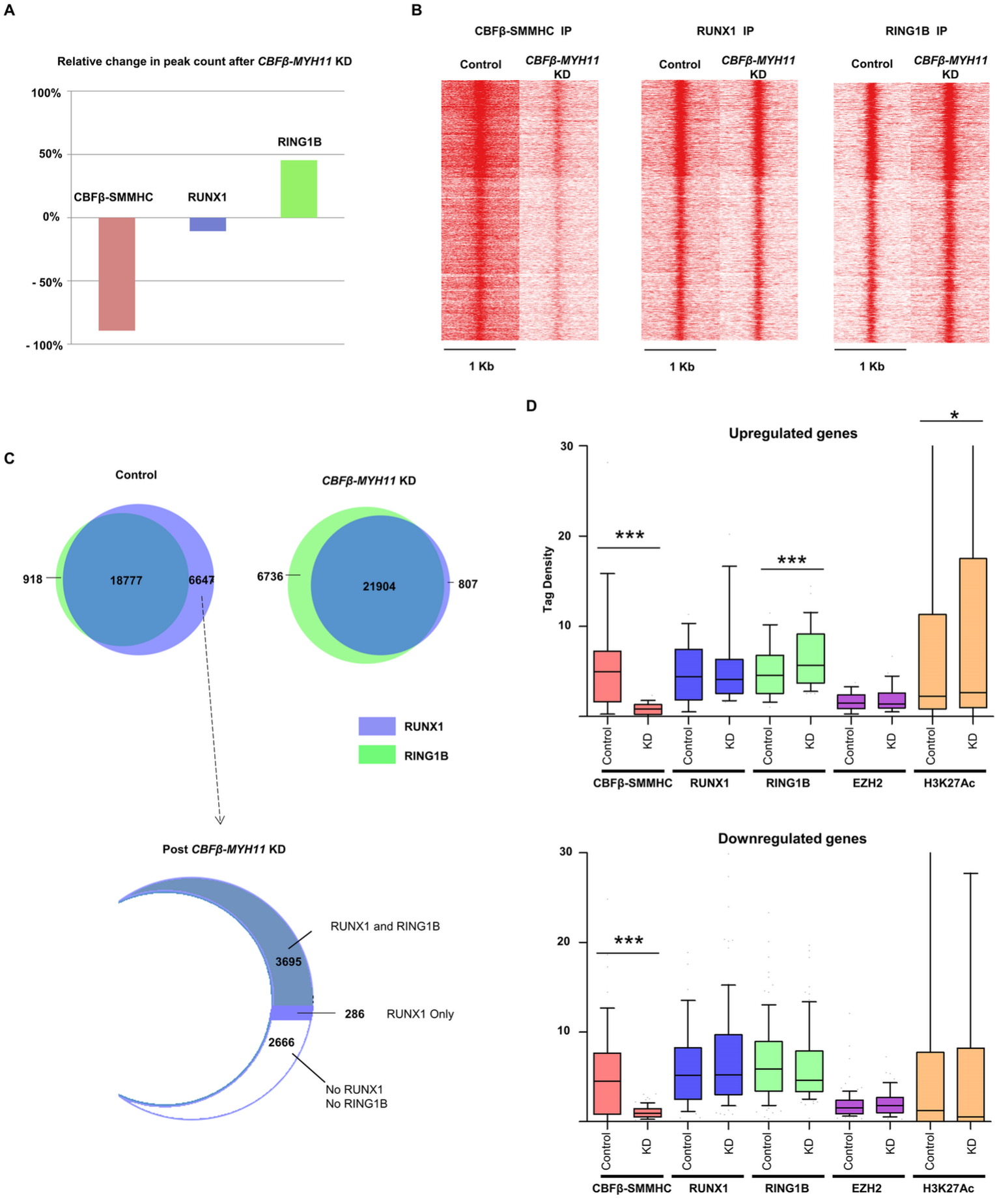
A
Relative change in peak count after CBFβ-MYH11 KD
100%
50%
0%
- 50%
- 100%
CBFβ-SMMHC
RUNX1
RING1B
B
CBFβ-SMMHC IP
RUNX1 IP
RING1B IP
Control
CBFβ-MYH11 KD
1 Kb
C
Control
CBFβ-MYH11 KD
918
18777
6647
6736
21904
807
RUNX1
RING1B
Post CBFβ-MYH11 KD
RUNX1 and RING1B
3695
286
RUNX1 Only
2666
No RUNX1
No RING1B
D
Upregulated genes
Downregulated genes
Tag Density
30
20
10
***
*
Control
KD
CBFβ-SMMHC
RUNX1
RING1B
EZH2
H3K27Ac

Figure 4

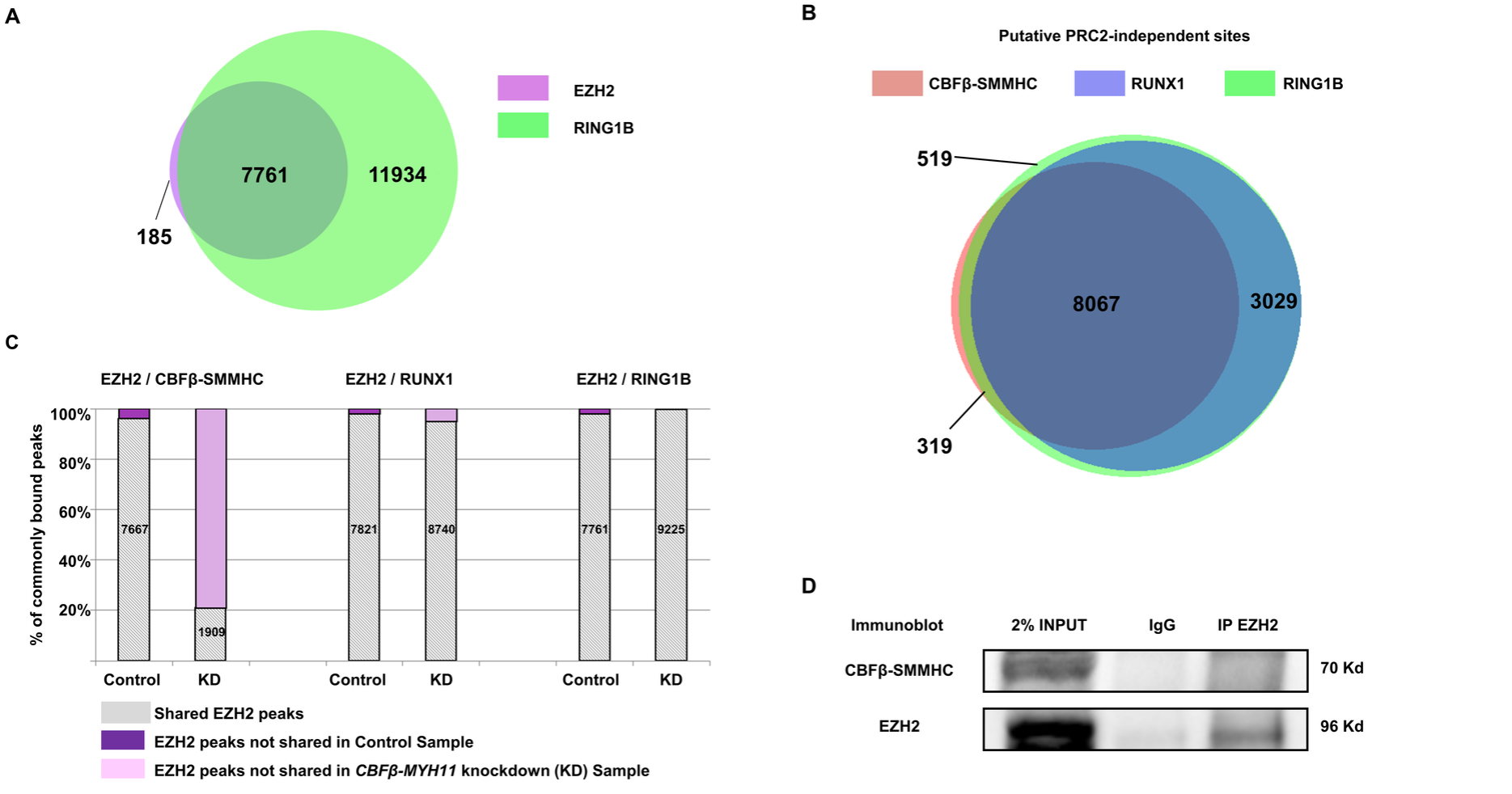
A
EZH2
RING1B
7761
11934
185
B
Putative PRC2-independent sites
CBFβ-SMMHC
RUNX1
RING1B
519
8067
3029
319
C
EZH2 / CBFβ-SMMHC
EZH2 / RUNX1
EZH2 / RING1B
% of commonly bound peaks
100%
80%
60%
40%
20%
7667
1909
7821
8740
7761
9225
Control
KD
Control
KD
Control
KD
Shared EZH2 peaks
EZH2 peaks not shared in Control Sample
EZH2 peaks not shared in CBFβ-MYH11 knockdown (KD) Sample
D
Immunoblot
2% INPUT
IgG
IP EZH2
CBFβ-SMMHC
70 Kd
EZH2
96 Kd

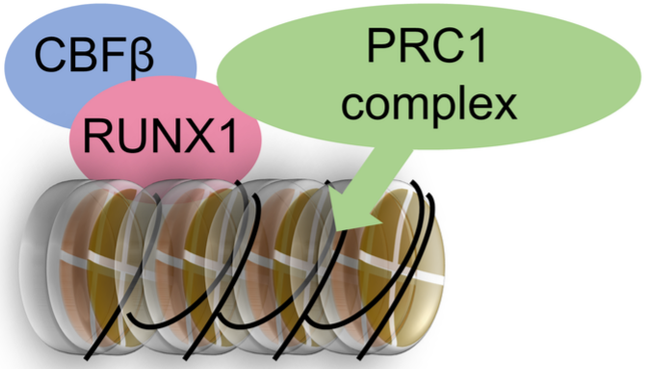

Wild-type CBF
Normal PRC1 recruitment

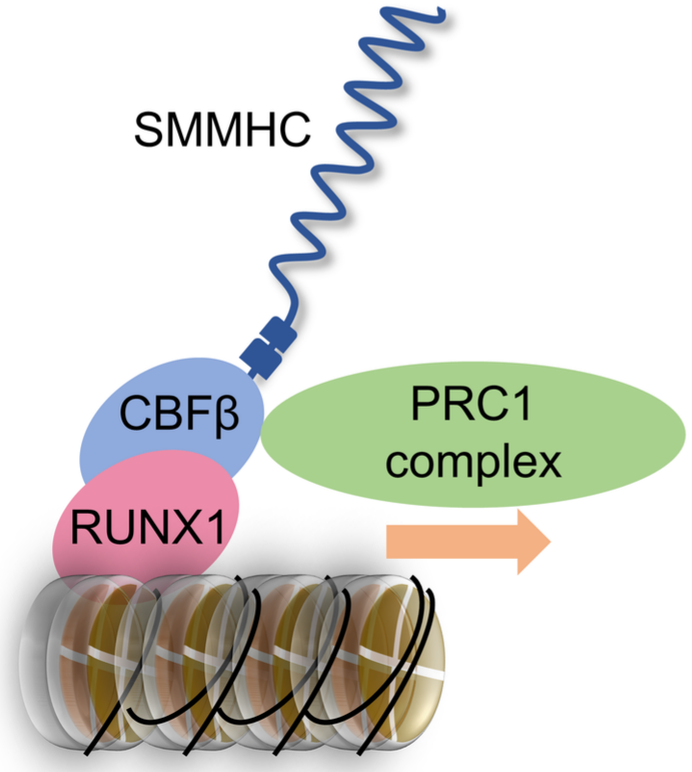

CBF fusion protein in AML
Altered PRC1 recruitment